Revealing the cosmic evolution of quasars using metallicity indicators

Ewa Skorek[1], Swayamtrupta Panda[2,3]

[1]University of Warsaw, Poland

[2]Center for Theoretical Physics, Polish Academy of Sciences, Warsaw, Poland

[3]Nicolaus Copernicus Astronomical Center, Polish Academy of Sciences, Warsaw, Poland

Abstract

Broad-band spectra of active galaxies contain a wide range of information that help reveal the nature and activity of the central continuum source and their immediate surroundings. Understanding the evolution of metals in the Active Galactic Nuclei (AGN) spectra and linking them with the various fundamental black hole (BH) parameters, for example, BH mass, the bolometric luminosity of the source, its accreting power, can help address the connection between the growth of the BH across cosmic time. We investigate the role of selected metallicity indicators utilizing the rich spectroscopic database of emission lines covering a wide range in redshift in the Sloan Digital Sky Survey's recent spectroscopic data release. We make careful filtering of the parent sample to prepare a pair of high-quality, redshift-dependent sub-samples and present the first results of the analysis here. To validate our findings from the simple correlations, we execute principal component analysis (PCA) over our sub-samples and present the 3D projection maps here which highlight the primary drivers of the observed correlations. The projection maps also allow us to isolate peculiar sources of potential interest.

Introduction

The chemical properties of galaxies have been considered as one of the key parameters in understanding galaxy evolution, one that is closely related to the star formation history (Maiolino & Mannucci 2019). Active galaxies, owing to their large luminosity range, can be observed over a broad range of redshift. An important constituent of the active galactic nuclei (AGN) are the broad-line region (BLR) - a conglomeration of gravitationally bound gas and metal rich media, that are primarily responsible for the broad emission lines observed in a typical AGN spectrum. A handful of diagnostic ratios in the UV and optical have been tested to study and constrain the metal content in the BLR, notable among them are the (i) N Vλ1240/C IVλ1549; (ii) Fe II(2700-2900Å)/Mg IIλ2800; hereafter Fe II(UV)/Mg II; and (iii) Fe II(4434-4684Å)/Hβλ4861; hereafter Fe II(opt)/Hβ (Hamann & Ferland 1992, Panda et al. 2019, Shin et al. 2021). The three diagnostic ratios probe the metal content of BLR at different redshift ranges and a possible link between them, if established, can allow to gain further insights in the AGN-host co-evolution across cosmic time.

Telescope, Observations, and Parent Sample

We start with the Rakshit et al. (2020) DR-14 QSO catalogue which contains a database of all the spectroscopically confirmed quasars observed during any SDSS data release, consisting of 526,356 quasars based on i-band absolute magnitude $M_i < -20.5$ and having at least one emission line with a full width at half maximum (FWHM) larger than 500 km s^{-1} (Pâris et al. 2018). Each spectrum is analyzed using the publicly available multi-component spectral fitting code `PYQSOFIT` (Guo et al. 2018). The full catalogue contains the continuum and line properties of several emission lines that cover the Hβ, Mg II, and C IV regions. From the derived emission line parameters, single-epoch virial black hole masses (M_{BH}) for the sample are estimated using Hβ, Mg II, and C IV emission lines. The sample covers a wide range in bolometric luminosity and black hole mass. This serves as our parent sample.

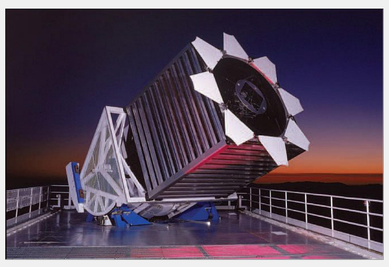

Figure 1: The Sloan Foundation 2.5m Telescope at Apache Point Observatory (New Mexico).

Distribution of fundamental BH parameters

In order to evaluate the efficacy of the aforementioned metallicity indicators that span a wide range in the redshift and keeping in mind the spectral coverage of SDSS (3600 - 10,400 Å), we prepare a pair of high-quality sub-samples: (A) a low-redshift sample ($0.617 \leq z \leq 0.89$) containing 6,072 sources that encompass the Fe II(UV), Mg II, Fe II(opt) and Hβ emission lines; and (B) a high-redshift sample ($2.09 \leq z \leq 2.25$) containing 1,950 sources that cover the N V, C IV, Fe II(UV) and Mg II emission lines. Two representative spectra, one from each sub-sample, are shown in Figure 2.

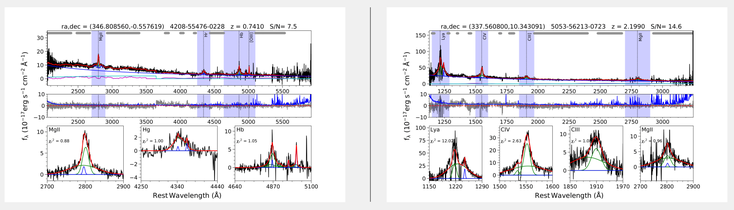

Figure 2: Exemplary AGN spectra from our (LEFT) low-z sample (SDSSJ223014.59+102035.1), (RIGHT) high-z sample (SDSSJ230714.05-003327.4).

We show the distribution of four basic properties of the AGN (redshift, bolometric luminosity (L_{bol}), BH mass and Eddington ratio - $\frac{L_{bol}}{L_{Edd}}$, where L_{Edd} is Eddington luminosity) for the sources in our two sub-samples relative to the parent sample (Figure 3). The compilation of statistical parameters for the sub-samples can be found in high-z sample and low-z sample.

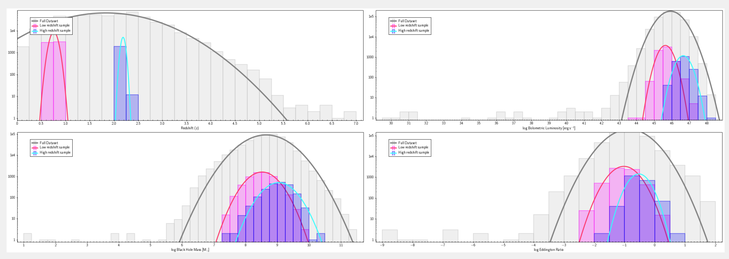

Figure 3: Distributions of the (a) redshift, (b) bolometric luminosity, (c) black hole mass, and (d) Eddington ratio, for the parent sample (in gray), low-z (in magenta) and high-z (blue) sub-samples.

"We confirm that the ratio of the EW of the Fe II blend in the UV (i.e. between 2700-2900 Å) to the EW of the broad Mg II, traces the bolometric luminosity and BH mass, and is a robust indicator of the quasar evolution across cosmic time."

Metallicity indicators and correlations

A physical connection between the Fe II(UV)/Mg II ratio and BLR metallicity can be understood in terms of metal enrichment from star formation. As a proxy of the Fe/Mg abundance ratio, we can track the change of Fe II(UV)/Mg II as a function of time from the onset of star formation based on an enrichment delay (tens of Myr to a few Gyrs, Matteucci & Recchi 2001) between α-elements and iron which are produced mainly from Type II and Type Ia supernovae, respectively (see Shin et al. (2021) for an overview). The correlation between several line flux ratios, tracing the chemical properties of the BLR, and Eddington ratio can be considered as the relation between the BLR metallicity and accretion activity of AGN. We consider here the Fe II(UV)/Mg II ratio but intend to extend the study to include other similar indicators in our analysis.

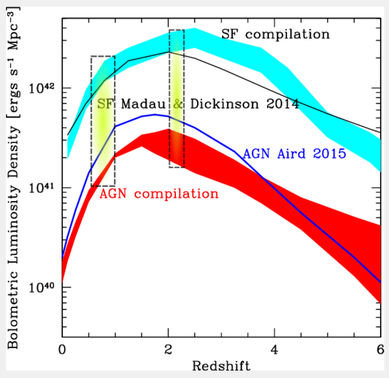

Figure 4: The evolution of the AGN bolometric luminosity density (Fiore et al. 2017): the red band has been computed from a compilation of X-ray luminosity functions integrated in the range log L_X = 42-45 and assuming the Marconi et al. (2004) bolometric correction; the blue solid line is the Aird et al. (2015) determination. The cyan band represents a compilation for the UV luminosity density. The black solid line is the Madau & Dickinson (2014) determination. The dashed boxes mark the redshift range of our two sub-samples.

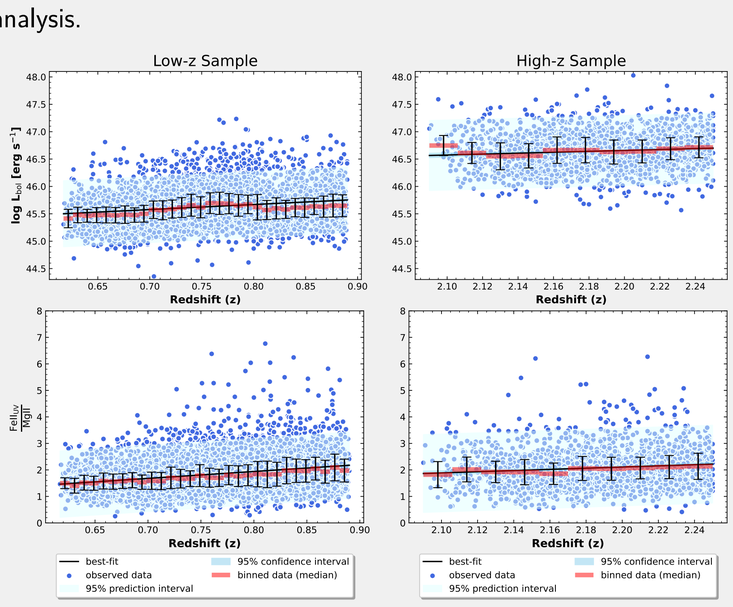

Figure 5: Upper panels show the bolometric luminosity distribution as a function of redshift for the (LEFT) low-z, (RIGHT) high-z sub-samples. We median-bin the data-sets accounting for the relative number of sources in each sub-sample. A linear-fit with 95% confidence and prediction intervals are also shown. Lower panels show the corresponding behaviour for the ratio Fe II(UV)/Mg II as a function of redshift.

From Figure 5 (upper panels) we can clearly notice the change in the gradient of the distribution - going from a steeper slope (~0.92) to a shallower one (~0.84), in addition to the rise in the net luminosity. These are consistent with the conclusions from prior works involving the study of evolution of quasar luminosity function and its similarity with the progression of star-formation rate density across cosmic time (see Figure 4). We confirm a similar behaviour for the ratio Fe II(UV)/Mg II (slope decreases from 2.61 to 2.22).

Principal Component Analysis (PCA)

Principal component analysis (hereafter PCA) is based on the eigenvalue decomposition method and inherently assumes the input variables to have no inter-dependency. PCA works by initially finding the principal axis along which the variance in the multidimensional space (corresponding to all recorded properties) is maximized. This axis is known as eigenvector 1. Subsequent orthogonal eigenvectors, in order of decreasing variance along their respective directions, are found, until the entire parameter space is spanned (see Abdi & Williams (2010), Martínez-Aldama et al. (2021), for a more in-depth review).

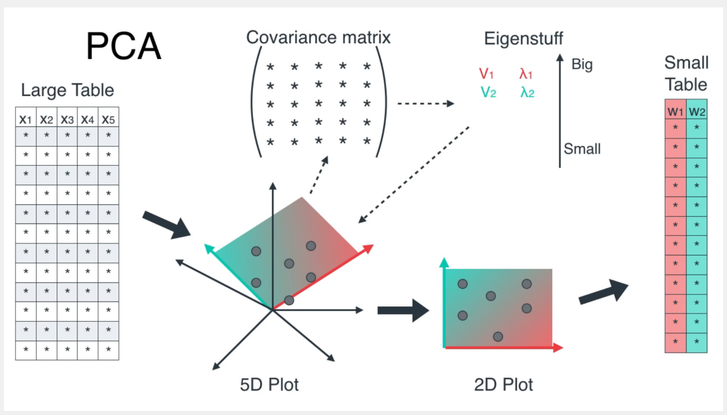

Figure 6: An illustration indicating the steps involved in the principal component analysis (PCA). Check this step-by-step walk-through to PCA.

What PCA reveals for our samples?

After standardizing our data-sets, we run the PCA utilizing five observables, each for the two sub-samples, obtained directly from the spectral fitting of the SDSS spectra. The results from the analysis are shown in Figure 7.

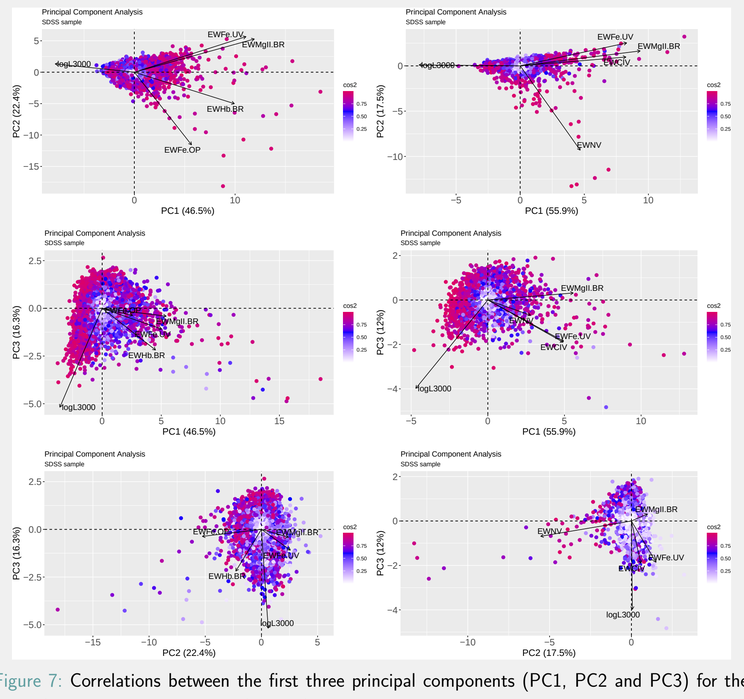

Figure 7: Correlations between the first three principal components (PC1, PC2 and PC3) for the (LEFT) low-z sub-sample, and (RIGHT) high-z sub-sample. The contribution of the respective principal components to the overall variance in the data-sets is also noted. The cos2 represents the contribution of the component to the squared distance of the data-point from the origin. The vectors denote the contribution of the selected observed parameters used as inputs for the PCA.

Highlights and future work

- We re-confirm the usability of Fe II(UV)/Mg II ratio as a robust indicator of the quasar evolution across cosmic time.
- Preliminary PCA results have supplemented the conclusions obtained from direct correlations. PCA analysis has provided indication of primary drivers of the sub-samples. It has also allowed us to gather peculiar sources. The analysis of the spectra of these sources in ongoing.
- We plan to experiment with other linear and non-linear clustering algorithms and benchmark their performances, and
- Address the physical mechanisms at play using radiative transfer modelling accounting for the change in the ionizing continuum across a wide range of redshift.

We thank Prof. Bożena Czerny (CFT-PAN) for her helpful suggestions and discussions. The project is funded by the National Science Center grant 2017/26/A/ST9/00756 (MAESTRO 9).